AD-A068 440 ROCKWELL INTERNATIONAL THOUSAND OAKS CALIF SCIENCE --ETC F/G 11/2
IMPACT DAMAGE THRESHOLDS IN BRITTLE MATERIALS IMPACTED BY WATER--ETC(U)
MAR 79 A G EVANS, Y M ITO, M ROSENBLATT N00014-75-C-0669
UNCLASSIFIED SC5023.11FR NL

1 OF 1
ADA
068440

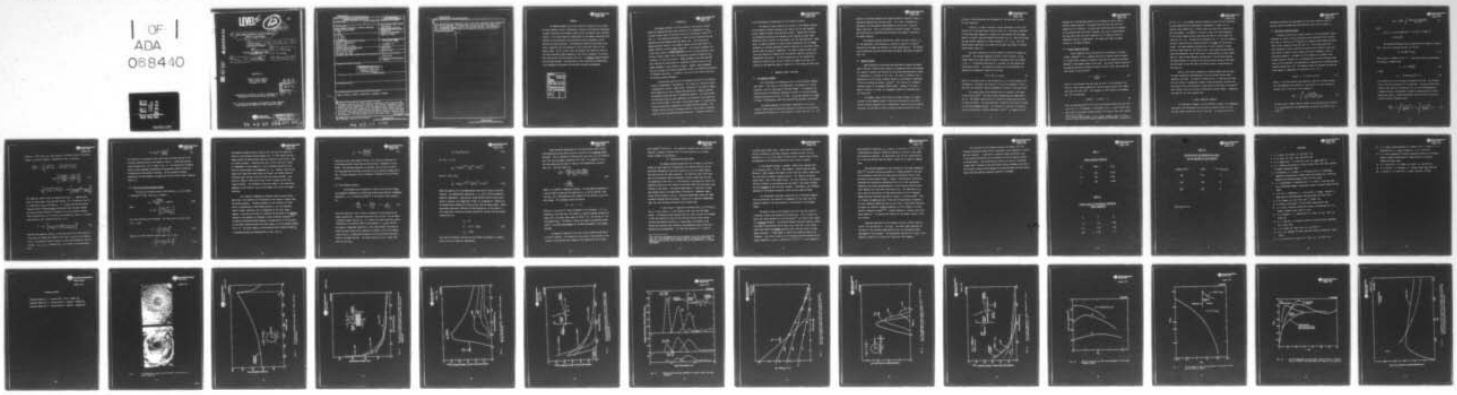

END
DATE
FILMED
6-79
DDC

LEVEL II

16

12 Sc

14 SC5023.11FR

6 IMPACT DAMAGE THRESHOLDS IN BRITTLE MATERIALS IMPACTED BY WATER DROPS.

9 Final Report. 1 Mar 75-31 Dec 78

03/01/75 thru 12/31/78

10 A. G. /Evans,
Y. M. /Ito,
M. /Rosenblatt

15 Contract No. N00014-75-C-0669
Project No. 471

11 Mar 79 12 40p.

Submitted to:

Office of Naval Research
800 N. Quincy Street
Arlington, VA 22217

This research was sponsored by the Office of Naval Research under Contract No. N00014-75-C-0669 (Project No. 471)

Science Center
Rockwell International

UNCLASSIFIED

SECURITY CLASSIFICATION OF THIS PAGE (When Data Entered)

REPORT DOCUMENTATION PAGE		READ INSTRUCTIONS BEFORE COMPLETING FORM
1. REPORT NUMBER	2. GOVT ACCESSION NO.	3. RECIPIENT'S CATALOG NUMBER
4. TITLE (and Subtitle) IMPACT DAMAGE THRESHOLDS IN BRITTLE MATERIALS IMPACED BY WATER DROPS.		5. TYPE OF REPORT & PERIOD COVERED Final Report 03/01/75 thru 12/31/78
		6. PERFORMING ORG. REPORT NUMBER SC5023.11FR
7. AUTHOR(s) A. G. Evans Y. M. Ito M. Rosenblatt		8. CONTRACT OR GRANT NUMBER(s) N00014-75-C-0669
9. PERFORMING ORGANIZATION NAME AND ADDRESS Rockwell International Science Center Thousand Oaks, CA 91360		10. PROGRAM ELEMENT, PROJECT, TASK AREA & WORK UNIT NUMBERS Project No. 471
11. CONTROLLING OFFICE NAME AND ADDRESS Office of Naval Research 800 N. Quincy Street Arlington, VA 22217		12. REPORT DATE March 1979
		13. NUMBER OF PAGES 37
14. MONITORING AGENCY NAME & ADDRESS(if different from Controlling Office)		15. SECURITY CLASS. (of this report) UNCLASSIFIED
		15a. DECLASSIFICATION/DOWNGRADING SCHEDULE

16. DISTRIBUTION STATEMENT (of this Report)

DISTRIBUTION STATEMENT A
Approved for public release;
Distribution Unlimited

17. DISTRIBUTION STATEMENT (of the abstract entered in Block 20, if different from Report)

18. SUPPLEMENTARY NOTES

19. KEY WORDS (Continue on reverse side if necessary and identify by block number)

Impact, erosion, ceramics, projectiles, toughness, hardness

20. ABSTRACT (Continue on reverse side if necessary and identify by block number)

The damage threshold for brittle materials impacted by water drops has been studied by using a combination of analytic and numerical approaches to obtain solutions for the impact stress fields and dynamic stress intensity factors. It has been shown that expressions for the damge threshold, which consists of the activation of pre-existent surface microcracks, can be derived from these solutions. The expressions identify three types of behavior, depending upon the adjacence of the pre-existent cracks to the impact center, vis-a-vis their
(continued)

DD FORM 1 JAN 73 1473 EDITION OF 1 NOV 65 IS OBSOLETE

UNCLASSIFIED

SECURITY CLASSIFICATION OF THIS PAGE (When Data Entered)

size, and describe the respective roles of the three important target parameters, the fracture toughness, the elastic wave velocity and the pre-existent flow size. An absolute damage threshold has also been defined. The conditions at this threshold are demonstrated to be reasonably consistent with available threshold measurements.

SUMMARY

The damage threshold for brittle materials impacted by water drops has been studied by using a combination of analytic and numerical approaches to obtain solutions for the impact stress fields and dynamic stress intensity factors. It has been shown that expressions for the damage threshold, which consists of the activation of pre-existent surface microcracks, can be derived from these solutions. The expressions identify three types of behavior, depending upon the adjacence of the pre-existent cracks to the impact center, vis-a-vis their size, and describe the respective roles of the three important target parameters, the fracture toughness, the elastic wave velocity and the pre-existent flaw size. An absolute damage threshold has also been defined. The conditions at this threshold are demonstrated to be reasonably consistent with available threshold measurements.

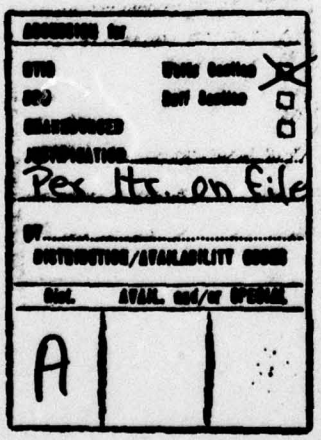

I. INTRODUCTION

The damage threshold in brittle materials (particularly ceramic materials) impacted by water drops consists of the propagation of pre-existent surface cracks to form well-defined circumferential cracks[1,2,3] (Fig. 1). The cracks are activated by a tensile pulse associated with the Rayleigh wave that emanates from the impact site. The initiation of damage typically occurs in the subsonic regime, and has been shown[2] to depend primarily on three target properties: the fracture toughness, the elastic wave velocity ($\sqrt{\text{modulus/density}}$) and the size distribution of pre-existent surface cracks; while the important projectile properties are, evidently, its size and velocity. Damage parameters have been derived[2] that indicate the trend toward an increasing threshold velocity as the target toughness or wave velocity increase. However, these parameters have not yet been sufficiently quantified to permit the effective prediction of threshold velocities. In addition, the role of the initial flaw size distribution remains ambiguous.

A quantitative definition of the damage threshold will ultimately require an experimental investigation. This study will inevitably entail a comprehensive series of impact tests: searching for the onset of damage. Before embarking on such a program some theoretical insights regarding the expected trends would be of considerable benefit. This would permit the efficient choice of test conditions and of materials that probe the most critical trends. The intent of the present paper is to develop the requisite quantitative approach to the damage threshold problem. The concept involves the use of selected numerical calculations as specific inputs to crack activation and growth analyses: ultimately leading to

to the development of expressions for the threshold velocity.

The numerical inputs required for analysis of the damage threshold are the dynamic stresses produced by the impact, and the time dependent stress intensity factors at pre-existent cracts[2]. Appropriate solutions are obtained by analyzing the response of ZnSe impacted by water drops. Normalized forms, suitable for more general use, are then described. Thereafter, an analytic approach is used to obtain expressions for the damage threshold, by invoking approximate analytic functions for the stress fields derived from the numerical computions. The stress intensity factor functions thus derived are compared with the specific numerical solutions to substantiate the results. The final expressions for the threshold are obtained in terms of the critical velocity for damage initiation, as a function of the important physical properties of the target and water drop.

2. NUMERICAL IMPACT SOLUTIONS

2.1 The Numerical Method

The calculations are conducted using a finite-difference computer code, WAVE-L. This code is a two-dimensional (axi-symmetric or planar), Lagrangian, explicit code based on the HEMP scheme[4]. It integrates the governing partial differential equations of motion for arbitrary dynamic problems concerned with solids or fluids. It has been applied to a number of impact investigations, under both subsonic[5] and hypersonic conditions[6].

The method employed in the present investigation is to use a pressure loading function previously obtained[7] by examining the pressures developed during impact of a rigid surface by a water drop (Fig. 2). This

function is pertinent whenever the surface deflection induced by impact is negligible compared with the drop radius. It is thus a reasonable approximation for high modulus target materials at low (e.g., subsonic) impact velocities. This is the condition of present interest. The pressure function p(r,t) specifies both the spatial and temporal features of the impact pressure.

The pressure function derived for a water drop with a radius, r_p, of 1 mm impacting a rigid surface at a velocity of 220 ms^{-1} is used to calculate the stresses that develop in a ZnSe target material. The results can be normalized using the dimensionless parameters described by Blowers[8] (Eqn. 16).

2.2 Impact Stresses

Some preliminary calculations were performed to examine the magnitude of the near surface stress gradient, by conducting stress calculations at a specific location (the position on the surface where the tensile stress is a maximum) as a function of cell size. The results, plotted in Fig. 3, demonstrate that the stress increases rapidly as the surface is approched: a result anticipated by Blowers' analysis[8]. This feature will become an important aspect of the damage threshold model. Because of the rapid spatial variation in stress, all subsequent studies are conducted using the finest grid.

The dynamic stress field results of primary interest for damage analyses are the temporal trends in the stress (particularly the radial tensile stresses responsible for circumferential cracks) at various spatial locations, and the spatial stress variations normal and parallel to the

surface at times approaching the development of the peak tensile stress (at that location).

Initially, in order to provide a useful perspective of the stress fields, loci of the peak radial tensile stress (i.e., the stress regardless of time) have been computed as a function of the distance from the impact center, at several locations beneath the surface (Fig. 4). Near the surface, the peak tension develops at a radial distance, $r \equiv \hat{r} = 0.2r_p$. But, the tension decays appreciably with depth and the peak value tends to displace toward larger values of r.

The stress gradients are of more specific interest for damage calculations[2]. The stresses computed at several radial locations, at the instant where the surface tension attains its maximum value, are plotted in Fig. 5. The gradient diminishes as r increases, as anticipated from the previous results. The stress distribution can be approximately expressed by an exponential relation of the form;

$$\sigma \sim \hat{\sigma}(r) \exp\left[-(z/z_0)\right] \qquad (1)$$

where $\hat{\sigma}$ is the peak stress at the surface and z_0 is a scale dimension that increases as r increases; the values of $\hat{\sigma}$ and z_0 are tabulated in Table I. Note that the exponential spatial dependence is typical of Rayleigh waves[9].

The second stress field characteristic of interest is the shape of the stress pulse[10]. The tensile pulse computations are summarized in Fig. 6. The primary tensile pulse is located at the Rayleigh wave front, as noted previously. The pulse decreases in amplitude and tends to broaden as the wave propagates outward. The broadening is possibly attributed to varying contributions from the longitudinal wave[10]: as suggested by the

tendency for a low amplitude tension to be retained to larger times at the more remote locations. The primary tensile pulses are relatively symmetric at all locations. The peak stress amplitude tends to decrease as the distance from the surface increases, but occurs at approximately the same time (given the radial location) for all depths at which an appreciable tension is experienced. The pulses also tend to broaden slightly as the depth increases.

2.3 Stress Intensity Factors

Stress intensity factor calculations are performed by inserting cracked elements[5,7] (i.e., elements that do not support tensile stresses or in-plane shear stresses) at specific locations and computing the stress gradient in the elements ahead of the crack. The stress intensity factor K* can then be derived by fitting the crack tip stress field, taken along the crack plane, to the relation[11]

$$\sigma = \frac{K}{(2\pi x)^{\frac{1}{2}}} + \sigma^{\circ} \qquad (2)$$

where x is the distance from the crack tip and σ° is the constant first term of a Taylor series expansion of the non-singular stress field components near the crack tip[11]. The procedure is facilitated by rearranging Eqn. (2) into the form,

$$\sigma(2\pi x)^{\frac{1}{2}} = \sigma^{\circ}(2\pi x)^{\frac{1}{2}} + K \qquad (3)$$

Then, by plotting $\sigma(2\pi x)^{\frac{1}{2}}$ vs $x^{\frac{1}{2}}$, K can be obtained directly from the intercept at $x^{\frac{1}{2}} = 0$. The method is illustrated in Fig. 7: used to obtain the peak value of the stress intensity factor $\hat{K}$ for each of four crack lengths,

*All K values refer to mode I, or K_I, values; because cracks in brittle materials under tension are usually observed to follow mode I trajectories.

at $r/\hat{r} = 1.5$. It is evident from the linearity at small $x^{\frac{1}{2}}$ that the method is quite appropriate for approximate K computations: except for the smallest crack length ($a/r_p = 0.0125$), where the crack has a dimension of just one element. The method is now used to obtain the time dependence of the stress intensity factor (excluding the smallest crack length) for cracks at $r/\hat{r} = 1.5$. The results are plotted on Fig. 8. The first feature to note is that the stress intensity factors are larger for the smaller cracks. The other important characteristic is that K reaches its peak value at larger times for the larger cracks, even though the peak tension along the prospective crack plane occurs at approximately the same instant (Fig. 6). Both of these features are explained in the following section. The former behavior is related to the stress gradient acting on the crack, and the latter to the time taken to develop a stress intensification at the crack tip.

Finally, the stresses computed at locations remote from the crack are used to establish the magnitude of the near surface stress relief created by the crack. The results, plotted on Fig. 9, show that the stress near the surface is appreciably reduced; thereby providing a rationale for the spacing of the circumferential cracks observed after water drop impact[1,3]. Note, however, that the stresses are enhanced at greater depths: suggesting the potential for crack instabilities.

3. CRACK FORMATION THRESHOLD

The incidence of damage in brittle materials appears to be adequately described by the requirement that the stress intensity factor K at pre-existent cracks reaches the critical value K_c[12]. The damage threshold is

analyzed by examining the development of the stress intensity factor at surface cracks and determining the conditions under which K reaches K_c.

3.1 The Stress Intensity Factor

Analyses of the stress intensity factor at finite stationary cracks subjected to a normal tensile stress pulse have indicated[13] that K varies with time, t; initially as $t^{\frac{1}{2}}$ and then as a damped sinusoid about the quasi-static stress intensity factor K_s[14] (Fig. 10). The initial motion of a crack subjected to such a rapidly oscillating stress intensity factor probably occurs by means of small advance and arrest increments, prior to continuous extension. The details of this behavior are ignored in the present analysis; instead, it is considered that the initial motion of the crack will be continuous, and described by a monotonically increasing stress intensity factor (Fig. 10). The function chosen to represent the time and crack length, a, dependence of K (plotted in Fig. 10) is:

$$(K/K_s)^2 = [1 + (\pi^2/4)\ (a/tc)]^{-1} \tag{4}$$

where c is the wave velocity (the Rayleigh velocity for surface cracks). For time dependent pulse profiles, a solution for K can be obtained by summing K due to each prior time increment,[10]

$$K(t_o) = \int_0^{K_s} \frac{(t_o - t)^{\frac{1}{2}} dK_s}{[t_o - t + (\pi^2/4)\ (a/c)]^{\frac{1}{2}}} \tag{5}$$

The quasi-static stress intensity factor can be obtained from the stress $\sigma(z,r)$ associated with the Rayleigh wave by applying the Green's function[2,14]

$$K_s(r) = 2\left(\frac{a}{\pi}\right)^{\frac{1}{2}} \int_0^a \frac{\sigma(z,r)\,[1 + F(z/a)]dz}{(a^2 - z^2)^{\frac{1}{2}}} \qquad (6)$$

where

$$F(z/a) = (1-z/a)\,[0.295(z/a)^2 + 0.77(z/a)^4 - 0.99(z/a)^6 + 0.51(z/a)^8]$$

The stress distribution $\sigma(z,r)$ obtained from the numerical results (Eqn. (1)) can be inserted into Eqn. (6) to give,

$$K_s = 2\hat{\sigma}\sqrt{a/\pi}\;\; I(a/z_o) \qquad (7)$$

where $I(a/z_o)$ is plotted in Fig. 11: a convenient analytic approximation for $I(a/z_o)$, is found to be;

$$I \simeq \pi/2\;\; \sqrt{1+(a/z_o)} \qquad (8)$$

so that

$$K_s \simeq \hat{\sigma}\,[\pi a/(1+a/z_o)]^{\frac{1}{2}} \equiv \alpha\hat{\sigma} \qquad (9)$$

This relation for K_s can be used in conjunction with Eqn. (5) to obtain $K(t_o)$ if the time variation of $\hat{\sigma}$ is prescribed. The pulse profiles predicted by the numerical calculations (Fig. 6) can be approximated by triangular pulses, characterized in terms of stressing rate $\dot{\sigma}_\ell$ and an unstressing rate $\dot{\sigma}_u$. Substituting these ratios into Eqs. (5) and (9) yields the stress intensity factor

$$\frac{K(t_o)}{\alpha} = \dot{\sigma}_\ell \int_0^{t_m} \left[\frac{t_o - t}{t_o + \beta - t}\right]^{\frac{1}{2}} dt + \dot{\sigma}_u \int_{t_m}^{t_o} \left[\frac{t_o - t}{t_o + \beta - t}\right]^{\frac{1}{2}} dt \qquad (10)$$

where $\beta = (\pi^2/4)\,(a/c)$, $t_m = \hat{\sigma}_m/\dot{\sigma}_\ell$ and $\hat{\sigma}_m$ is the peak value of the surface stress at the crack location. Integration of Eqn. (10) gives;

$$\frac{K(t_o)}{\alpha} = \dot{\sigma}_\ell \left\{ \sqrt{t_o^2 + \beta t_o} - \sqrt{(t_o - t_m)^2 + \beta(t_o - t_m)} + \beta \ell n \left[\frac{\sqrt{t_o - t_m + \beta} + \sqrt{t_o - t_m}}{\sqrt{t_o + \beta} + \sqrt{t_o}} \right] \right\} \qquad (11)$$

$$- \dot{\sigma}_u \left\{ \sqrt{(t_o - t_m)^2 + \beta(t_o - t_m)} + \beta \ell n \left[\frac{\sqrt{\beta}}{\sqrt{t_o - t_m + \beta} + \sqrt{t_o - t_m}} \right] \right\}$$

The numerical results (Fig. 6) indicate that $\dot{\sigma}_\ell/\dot{\sigma}_u \sim 1$. Applying this ratio of stress rates, $K/\hat{\sigma}_m\alpha$ derived from Eqn. (11) is plotted in Fig. 12, as a function of t_o/t_m, for several β. It is noted that the peak stress intensity factor $\hat{K}$ develops <u>after</u> the maximum stress has been reached, and that the time differential increases as the crack length increases. These characteristics are in accord with the numerical results. An approximate expression for $\hat{K}$ obtained from Fig. 12 is;

$$\hat{K} \approx \hat{\sigma}_m \left[\frac{\pi a}{(1 + a/z_o)\,[1 + (\pi^2/4)\,(a\dot{\sigma}_\ell/c\hat{\sigma}_m)]} \right]^{1/2} \qquad (12)$$

Note that the quantity, $a\dot{\sigma}_\ell/c\hat{\sigma}_m$, is just the ratio of the time taken for a stress wave to traverse the length of the crack, $t_c (\equiv a/c)$ to the loading time t_ℓ. The numerical results (Section 2) have been obtained for the conditions $a > z_o$, $t_c \approx t_\ell$, whereupon Eqn. (12) reduces to the approximate form:

$$\hat{K} \sim 2(\hat{\sigma}_m)^{3/2} \left[\frac{z_o c}{\pi a \dot{\sigma}_\ell}\right]^{\frac{1}{2}} \tag{13}$$

The trend for $\hat{K}$ to decrease as the crack length increases was one of the principal characteristics of the numerical results. A more detailed comparison based on Eqn. (12) is shown in Fig. 13. The quantitative correspondence is quite reasonable considering the approximate nature of both the calculations and the analytic functions. We now procede to develop expressions for the threshold, by equating $\hat{K}$ to the critical stress intensity factor, K_c.

3.2 The Critical Crack Extension Stress

The value of the peak stress at the threshold, σ_c, can be found by equating $\hat{K}$ in Eqn. (12) to K_c, to obtain;

$$\sigma_c = \frac{K_c \sqrt{1+a/z_o}}{\sqrt{\pi a}} \cos(\phi/3) \tag{14a}$$

where

$$\phi = \cos^{-1}\left[\frac{7.5\dot{\sigma}_\ell a^{3/2}}{K_c c\sqrt{1 + a/z_o}}\right]$$

Two limit solutions are of interest. For long relative loading times ($c\sigma_c >> a\dot{\sigma}_\ell$),

$$\sigma_c \sim K_c \left(\frac{1 + a/z_o}{\pi a}\right)^{1/2} \tag{14b}$$

whereas, for short relative loading times ($c\sigma_c << a\dot{\sigma}_\ell$);

$$\sigma_c \sim \left[\frac{\pi(1 + a/z_o)\, K_c^2\, \dot{\sigma}_\ell}{4c}\right]^{1/3} \tag{14c}$$

The effective loading time will tend to vary with both the impact condition and the distance from the impact site. At sites remote from the impact center the loading times tend to be relatively long and Eqn. (14b) will tend to pertain: indicating that the critical stress will either be independent of crack length ($a >> z_o$) or decrease according to the familiar inverse square root dependence ($a < z_o$). However, close to the impact site, where the stress levels are larger, the loading times are relatively small and Eqn. (14c) will tend to be more pertinent: suggesting a regime in which the critical stress increases as the crack length increases. The influence of the crack length is thus sensitively dependent on the location, vis-a-vis the impact site, and on the impact condition.

For a material subjected to coninuous impact by water drops, each crack in the material will be exposed to wide range of loading times and stress gradients. A detailed analysis of the threshold will thus entail a determination of the minimum possible σ_c (for the specified range of impact conditions) and its dependence on the crack length. However, it may also be of merit to recognize the existence of an <u>absolute</u> minimum in the threshold (as observed in other threshold problems)[15,16]. An absolute threshold pertains whenever a maximum exists in the variation of the stress intensity factor with crack length, as in the present problem (Fig. 13). The crack length a_c at the maximum stress intensity factor $\hat{K}_m$ is obtained directly by differentiation of Eqn. (12) as,

$$a_c = \frac{2}{\pi} \left(\frac{z_o c \hat{\sigma}_m}{\dot{\sigma}_\ell} \right)^{\frac{1}{2}} \qquad (15)$$

Insertion of this crack length into Eqn. (12) yields an expression for the minimum possible stress that can be tolerated, independent of crack length. The resultant expression is unwieldy, and can only be used to full advantage when functional relations for $z_o(r)$ and $\dot{\sigma}_\ell(r)$ become available. Further discussion of this threshold is deferred to the following section.

3.3 The Threshold Velocity

The threshold can be expressed in terms of the critical target and projectile parameters by invoking the dimensionless material independent quantities T, Z, P, utilized by Blowers[8] in his analytic stress analysis, viz.

$$T = \frac{2c_t^2 t}{(rv)_p}, \quad Z = \frac{2(cz)_t}{(rv)_p}, \quad \Omega = \frac{\sigma_t}{(\rho cv)_p}. \qquad (16)$$

where the subscripts p and t refer to properties of the projectile and target respectively. Inserting these quantities into Eqn. (14) we obtain a threshold impact velocity v_p^c. It is found that three conditions prevail, determined by the relative values of the quantity $\zeta = r_p v_p / ac$ and the two material independent quantities T_L (the dimensionless time taken to attain the peak stress at the location of interest vis-a-vis the impact center) and Z_0 (a dimensionless measure of the sub-surface stress gradient at the same location). The three results are; for ζ larger than both $2/T_L$ and $2/Z_o$,

$$v_p^c \sim \hat{\Omega}\,(K_c/\sqrt{a})_t(\rho c)_p^{-1}\ , \tag{17a}$$

for $2/T_L < \zeta < 2/Z_o$,

$$v_p^c \sim (2/\pi Z_o \hat{\Omega}^2)^{1/3}\ (K_c^2)_t^{1/3}\ (rc^2\rho^2)_p^{1/3} \tag{17b}$$

and for $\zeta < 2/T_L,\ 2/Z_o$,

$$v_p^c \sim (\pi/Z_o T_L\ \hat{\Omega}^2)^{1/4}\ (K_c^2 c^3 a)_t^{1/4}\ (rc\rho)_p^{-1/2} \tag{17c}$$

Where the quantity $\hat{\Omega}$ is the dimensionless peak tensile stress at the flaw location. The dimensionless quantities, T_L, Z_o and $\hat{\Omega}$, can be obtained by numerical computation. Some typical values derived from the results presented in Section 2 are summarized in Table II, expressed as a function of the dimensionless distance $R(=2(cr)_t/(rv)_p)$ from the impact center. Highly approximate functional relations for these quantities, in the range $R > 7$ (the range where fractures are usually observed[2]), derived from the present computations are;

$$\begin{aligned} T_L &\sim 30 \\ \hat{\Omega} &\sim 2.2\ (1 - R/22) \\ Z_o &\sim 0.08R \end{aligned} \tag{18}$$

More precise functional relations can be evidently developed by a comprehensive series of numerical computations.

These functional expressions for the dimensionless impact stress field quantities can be used to obtain a relation for the absolute damage threshold. This is achieved by inserting the crack size a_c at the threshold Eqn. (15) into the general expression for $\hat{K}$ (Eqn. 12), equating $\hat{K}$ to K_c and then expressing the result in terms of the dimensionless variables (Eqn. 16). The final result is;

$$(v_p^c)^3 = \frac{2(K_c^2 c)_t \left[1 + (2/\pi)\sqrt{T_L/Z_o}\right]}{\hat{\Omega}_m^2 \, (Z_o T_L)^{1/2} \, (r\rho^2 c^2)_p} \tag{19}$$

$$\equiv \lambda \frac{(K_c^2 c)_t}{(r\rho^2 c^2)_p}$$

where λ is a material independent constant. The approximate magnitude of λ can by found by inserting the quantities T_L, Z_o and $\hat{\Omega}_m$ from Eqn. (18) into Eqn. (19), differentiating with respect to R and setting to zero for the minimum. This procedure yields the result;

$$R^* \sim 10, \quad \lambda \sim 1.4$$

where R^* is the value of R that corresponds to the threshold. It is interesting to note that Eqn. (19) predicts an absolute damage threshold for impact with 1 mm radius water drops of 128 ms^{-1} for ZnS and 504 ms^{-1} for hot pressed Si_3N_4. The former is within the range of experimental observation[17], providing encouragement for further development of the present approach.

The physical location of the crack at the threshold condition R^* is also of interest. This location is very close in each instance to the location of the maximum crack length for ZnS impacted by 250 μm radius

Nylon spheres[18] (Table III). This comparison suggests that the specified location is indeed a preferred site for crack extension, and provides further credence to the approach.

4.0 DISCUSSION AND CONCLUSIONS

The damage threshold associated with the impact of a brittle surface by water drops has indicated that the threshold velocity v_p^c has three forms, depending on the crack location vis-a-vis the impact center, the crack size and the impact condition. The conditions under which each form of the threshold should be expected to pertain depend upon the relative magnitude of the ratio, ζ, of the product of the projectile radius and projectile velocity to the product of the crack length and the elastic wave velocity in the target. The specific magnitudes of ζ required to invoke each regime relate to the magnitudes of the material independent impact stress field variables T_L and Z_o. Taking the approximate values for these variables obtained from the present, limited set of numerical computations (Eqn. 18), the following conclusions can be established.

A 'quasi-static' regime exists whenever both $r_p \tilde{>} 0.07\ a(c_t/v_p)$ and $r_t \tilde{>} 12.5a$, where r_t is the distance of the crack from the impact center. This behaviour thus pertains when the cracks are small with respect to both the projectile radius and the distance from the impact center and when the projectile velocity is large enough with respect to the elastic wave velocity that relatively large absolute values of the pulse duration can be established*. The crack then behaves as if it were in

*This velocity requirement derives from Blowers' result for normalized time (Eqn. 16). This normalization ignores some of the complexities of the contact process and may not, upon more detailed examination, be a stringent requirement.

a uniform, quasi-static field. Under these conditions, the threshold velocity increases as the target toughness increases and the flaw size decreases (i.e., as $K_c/\sqrt{a}$, typical of quasi-static, uniform stress fields), and decreases as the projectile density or wave velocity increase.

At the opposite extreme, a 'dynamic' regime exists whenever both $r_p \tilde{<} 0.7a(c_t/v_p)$ and $r_t \tilde{<} 12.5a$. This behavior prevails when the pulse duration is small enough with respect to the stress wave transit time across the crack that the dynamic response prevails. This requires relatively large cracks, close to the impact center. For such conditions, the threshold velocity increases as the toughness and wave speed in the target increase, and also <u>increases</u> as the flaw size increases. Additionally, the threshold decreases as the projectile density, radius and wave speed increase.

For intermediate conditions, where only one of the above inequalities are satisfied, the threshold is independent of the crack size, but otherwise depends on the same vaiables as the threshold in the dynamic regime.

The general trend in the threshold with crack size thus exhibits increasing, constant and decreasing characteristics. This is typical behavior for cracks subjected to stress gradients[15], and leads to the concept of an <u>absolute</u> threshold. The absolute threshold pertains whenever a broad size range of pre-existent micro-cracks exist, such that a crack always exists that yields the <u>maximum</u> possible stress intensity factor for each impact situation. A large number of impacts are needed to observe this threshold. The critical velocity at the absolute threshold depends on two target properties, K_c and c_t, according to $K_c^{2/3} c_t^{1/3}$. It also depends on

three projectile properties, r_p, ρ_p and c_p, in the form, $r_p^{-1/3}\rho_p^{-2/3}c_p^{-2/3}$. A proportionality constant relates the threshold velocity to these target and projectile properties. An approximate value for this proportionality of 1.4 has been derived from the present limited set of numerical computations.

The predicted dependence of the threshold on the target properties, $K_c^{2/3}c_t^{1/3}$, has been previously proposed as a damage parameter[2], and shown to be reasonably consistent with some sparse experimental data on crack activation by Nylon sphere impacts. However, interpretation difficulties concerned with asigning the appropriate value for K_c were encountered, especially with coarse grained materials in which the pre-existent microcrack lengths are on the order of the grain size. The importance of K_c and c_t and the implications for fabricating materials with an enhanced damage tolerance have been discussed at length in a previous paper[2]. Here it is merely re-emphasized that a fine-scale microstructure is essential, and that toughening mechanisms that do not invoke a large process zone must be sought; an important toughening mechanism in this category is the martensitic toughening process[19,20]. Surface compression stresses should also prove beneficial: by reducing the intensity of the impact stresses in the near surface.

Absolute predictions of the threshold velocity indicate values of 128 ms^{-1} for ZnS and 504 ms^{-1} for Si_3N_4. The former seems reasonable on the basis of the available damage data for ZnS, and encourages further development of this approach. The considerable superiority of Si_3N_4 is also apparent, primarily by virtue of its relatively high toughness.

The solutions for the threshold velocity now appear to be sufficiently quantitative that critical experiments can be designed to investigate the threshold. In particular, projectile impact conditions close to the predicted threshold can be selected to critically examine effects of microstructure. The microstructural effects can then be interpreted through their influence on the near-surface fracture toughness and elastic wave velocity: coupled with influences of the pre-existent crack size distribution when the absolute threshold condition is exceeded.

TABLE I

STRESS GRADIENT PARAMETERS

$r/\hat{r}$	$\hat{\sigma}$(MPa)	z_o/r_p
1	500	0.015
1.5	340	0.025
2	230	0.030

TABLE II

TYPICAL VALUES OF THE MATERIAL INDEPENDENT IMPACT PARAMETERS

R	$\hat{\Omega}$	Z_o
7.5	1.43	0.56
11.2	0.97	0.93
14.9	0.66	1.11

TABLE III

THE LOCATION OF THE MAXIMUM CRACK LENGTH
FOR ZnS IMPACTED BY NYLON SPHERES[18]

Velocity (ms^{-1})	r_t(μm)	$R^* = 2c_t r_t / r_p v_p$
406	100	8
633	200	10
1000	400	13

Calculated $R^* \sim 10$

REFERENCES

1. W. F. Adler, Jnl. Mater. Sci. 12 (1977) 1253
2. A. G. Evans, Jnl. Appl. Phys. 49 (1978) 3304
3. F. P. Bowden and J. E. Field, Proc. Roy. Soc. A282 (1965) 321
4. M. L. Wilkens, Calculation of Elastic-Plastic Flow, UCRL-7322, Lawrence Livermore Laboratory (1969)
5. M. Rosenblatt, G. E. Eggum, L. A. De Angelo and K. N. Kreyenhagen, 'Numerical Investigations of Water Drop Erosion Mechanisms' California Research and Technology Report, AFML-TR-76-193 (1976)
6. K. N. Kreyenhagen, M. Rosenblatt and T. R. Isbelle, 'Cratering, Mass Loss and Residual Damage in Hypersonic Impact' CRT Report AFML-TR-75-184 (1976)
7. Y. M. Ito, M. Rosenblatt, F. V. Perry and G. E. Eggum, 'Analysis of Water Drop Erosion Mechanisms' CRT Report AFML-TR-77-219 (1977)
8. R. M. Blowers, Jnl Inst. Math. Appl. 5 (1969), 167
9. H. Kolsky, Stress Waves in Solids (Dover Publications) 1963
10. A. G. Evans, Treatise on Materials Science and Technology (Ed. C.M. Preece), Academic Press (1979) in press.
11. M. A. Schroedl, J. J. McGovan and C. W. Smith, Jnl Exp. Mech. 14 (1974) 392
12. B. R. Lawn and T. R. Wilshaw, Fracture of Brittle Solids (Cambridge Univ. Press) 1975
13. L. B. Freund, Jnl. Mech. Phys. Vol. 21 (1973) 47
14. G. C. Sih, Handbook of Stress Intensity Factors, Lehigh Univ. Press (1973)
15. B. R. Lawn and A. G. Evans, Jnl. Mater. Sci., 12 (1977) 2195

16. F. F. Lange, Fracture Mechanics of Ceramics (Ed R. C. Bradt, D. P. H. Hasselman and F. F. Lange) Plenum, N.Y., vol 2 (1974) 599

17. W. F. Adler,'Response of Infrared Transparent Materials to Raindrop Impact', Effects Technology Inc. Report CR79-611 on contract F33615-78-C-5143 (1979)

18. A. G. Evans and T. R. Wilshaw, Jnl. Mater. Sci. 12 (1977) 97

19. R. C. Garvie, R. H. Hanninck, R. T. Pascoe, Nature 263 (1975) 703

20. D. Porter, A. G. Evans and A. H. Heuer, Acta Met. in press

TECHNICAL REPORTS

Technical Report No. 1 - Period 03/75 - 01/76 - SC5023.3TR

Technical Report No. 2 - Period 01/01/76 - 10/30/76 - SC5023.9TR

Technical Report No. 3 - Period 01/01/77 - 09/30/77 - SC5023.10TR

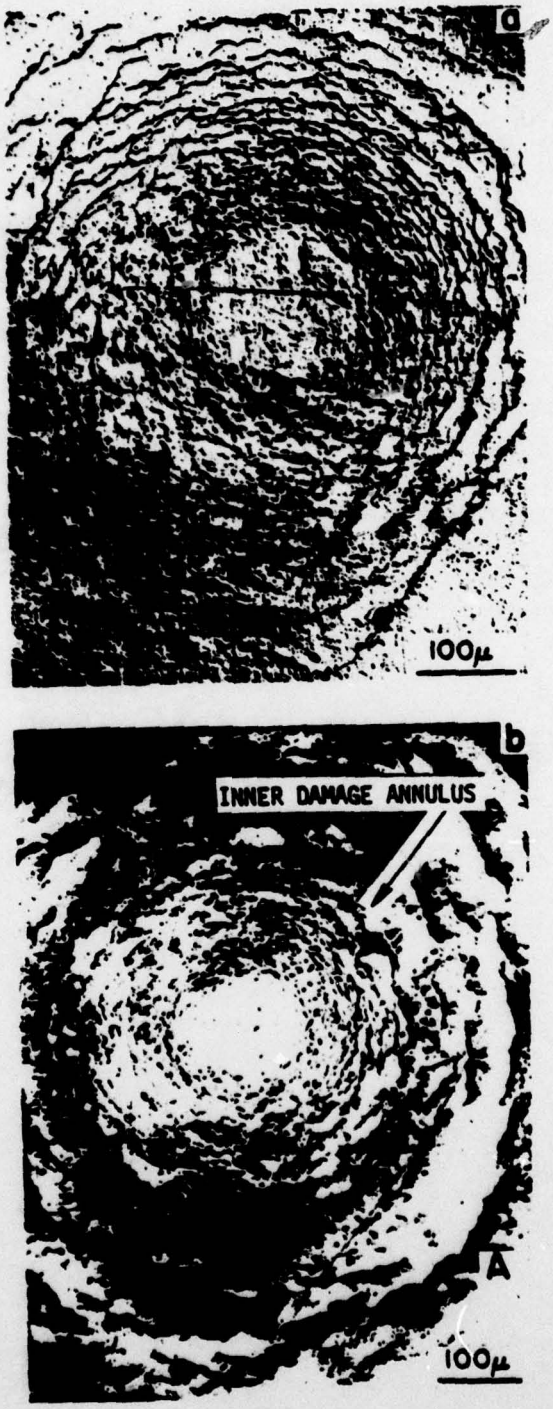

Fig. 1: Circumferential cracks on ZnS formed by the impact of a Nylon projectile.

Fig 1

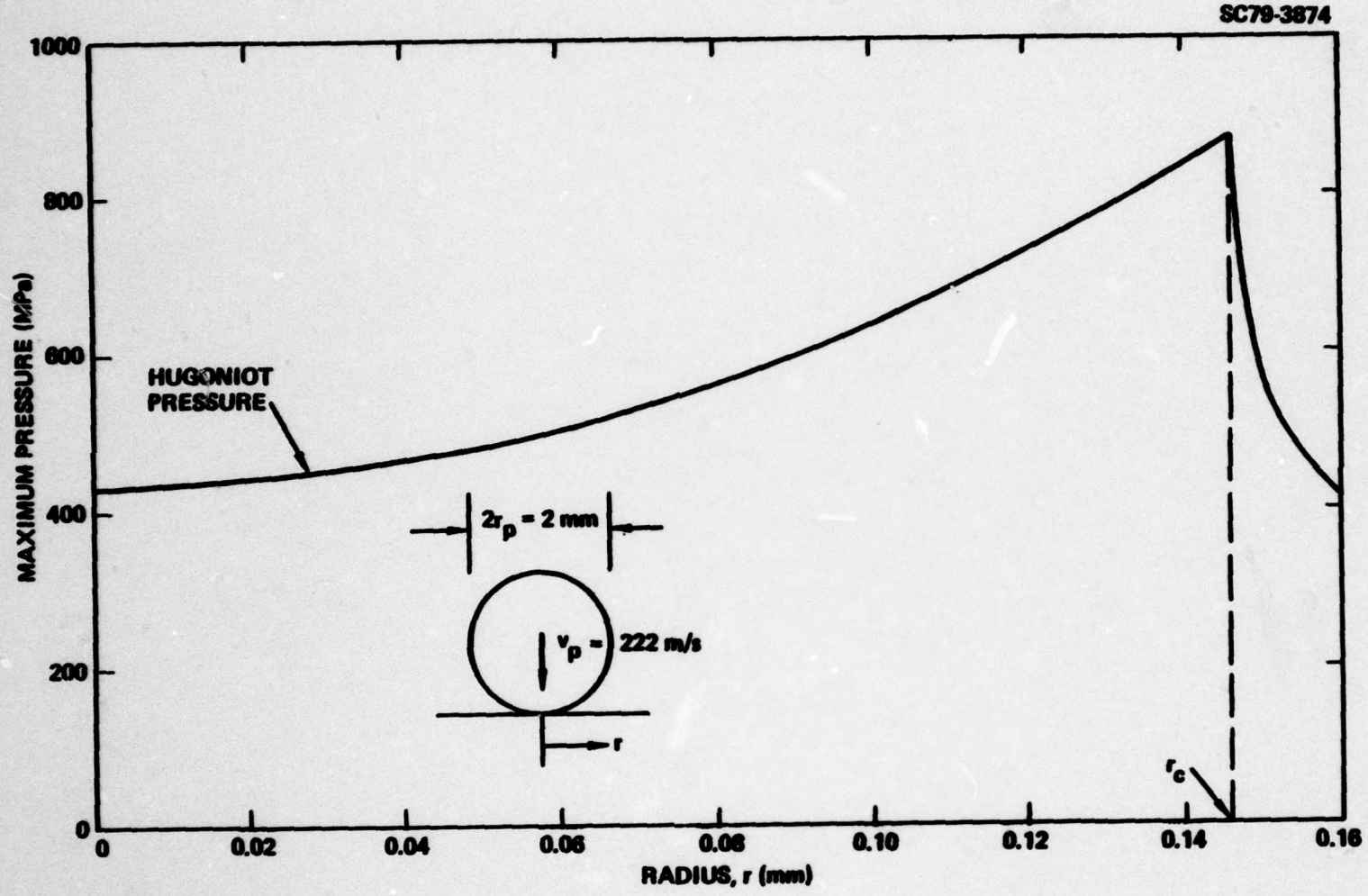

Fig. 2: The pressures developed during impact of a water drop onto a rigid surface.

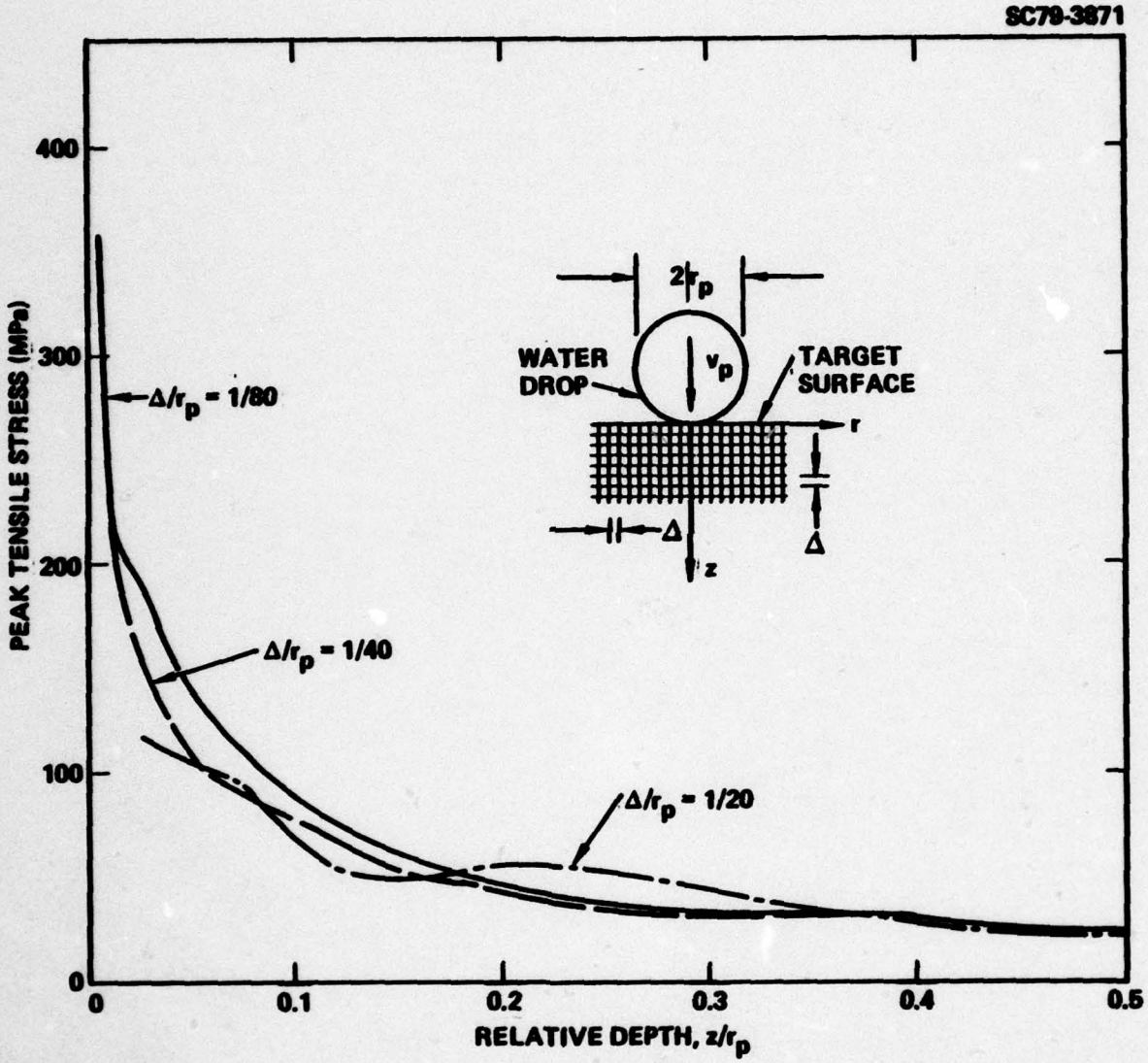

Fig. 3: The stress distribution beneath the surface at the location of peak near surface tension, obtained for three grid dimensions.

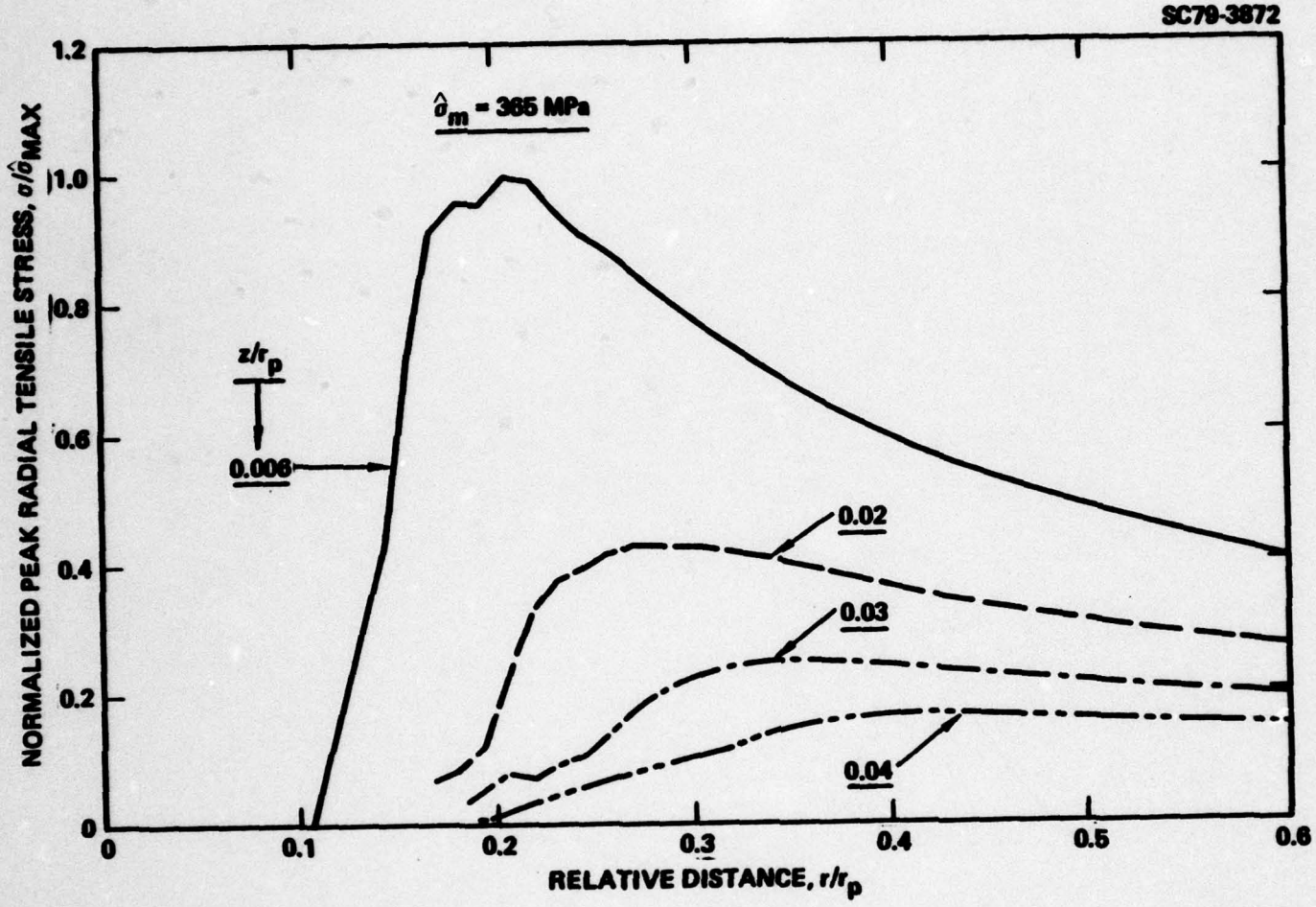

Fig. 4: Loci of the peak tensions, obtained for several planes beneath the surface.

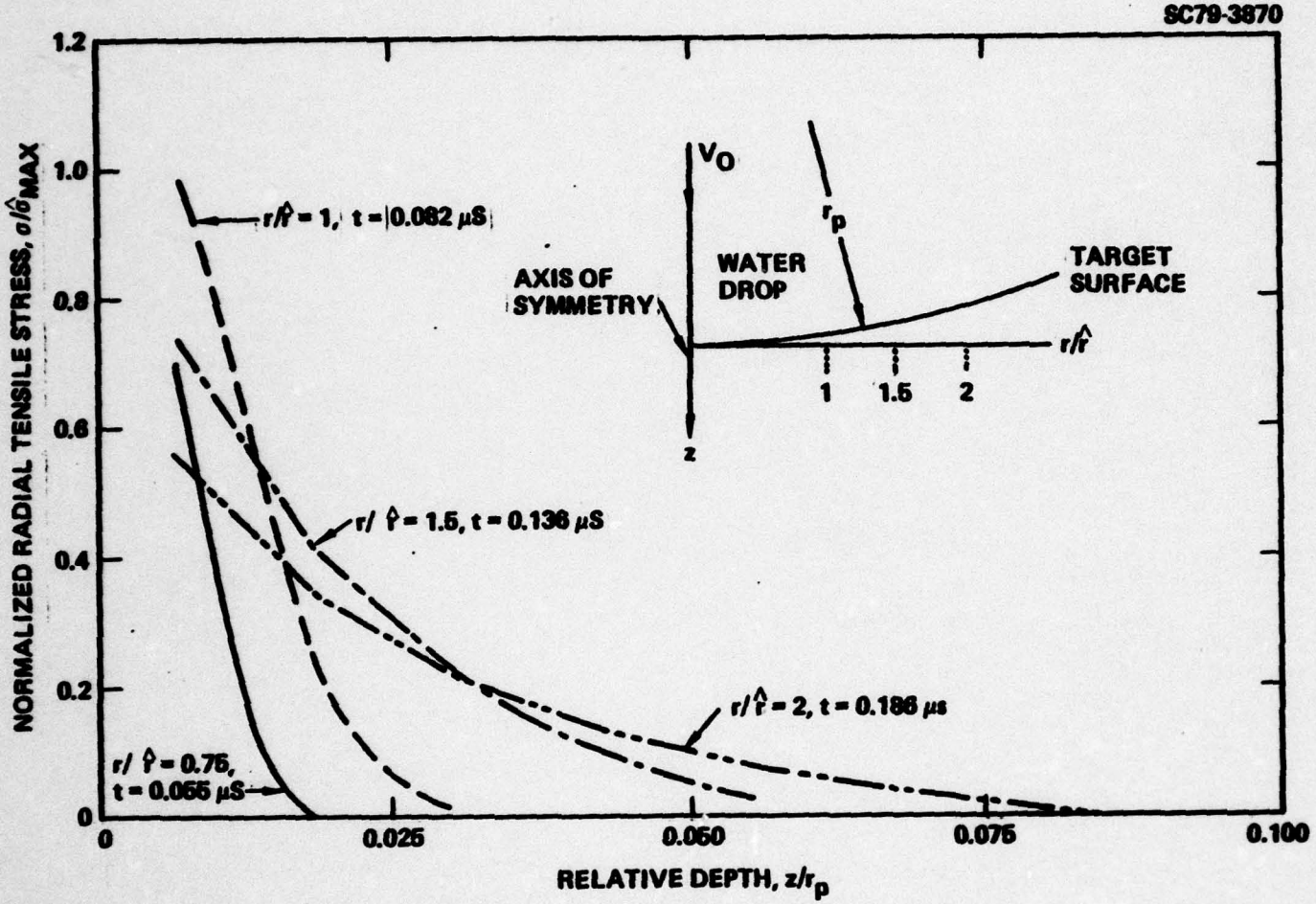

Fig. 5: The stress gradients at several radial locations, at the instants when the surface stress at each location attains its maximum value.

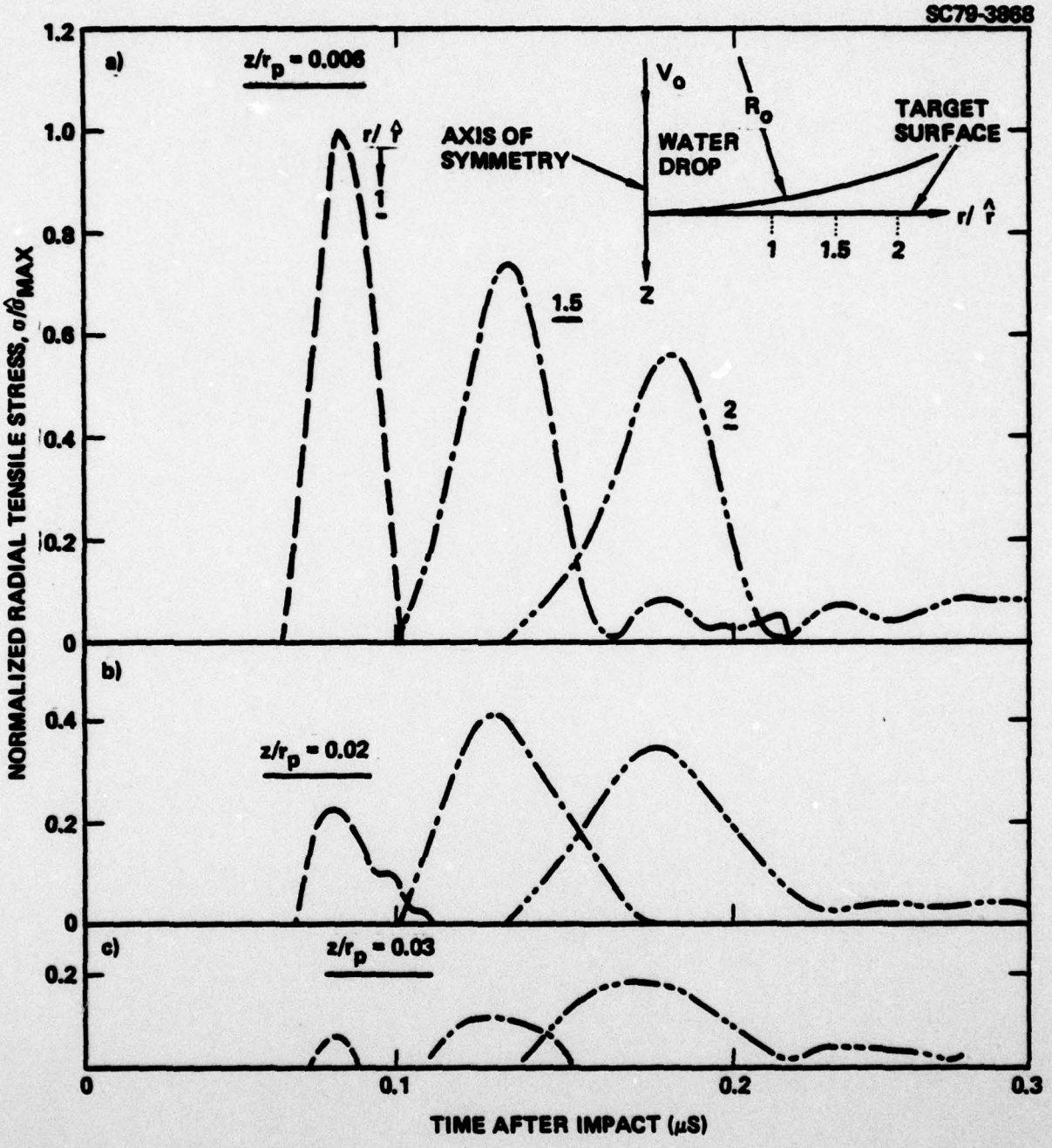

Fig. 6: Tensile pulse profiles computed at several radial and axial locations.

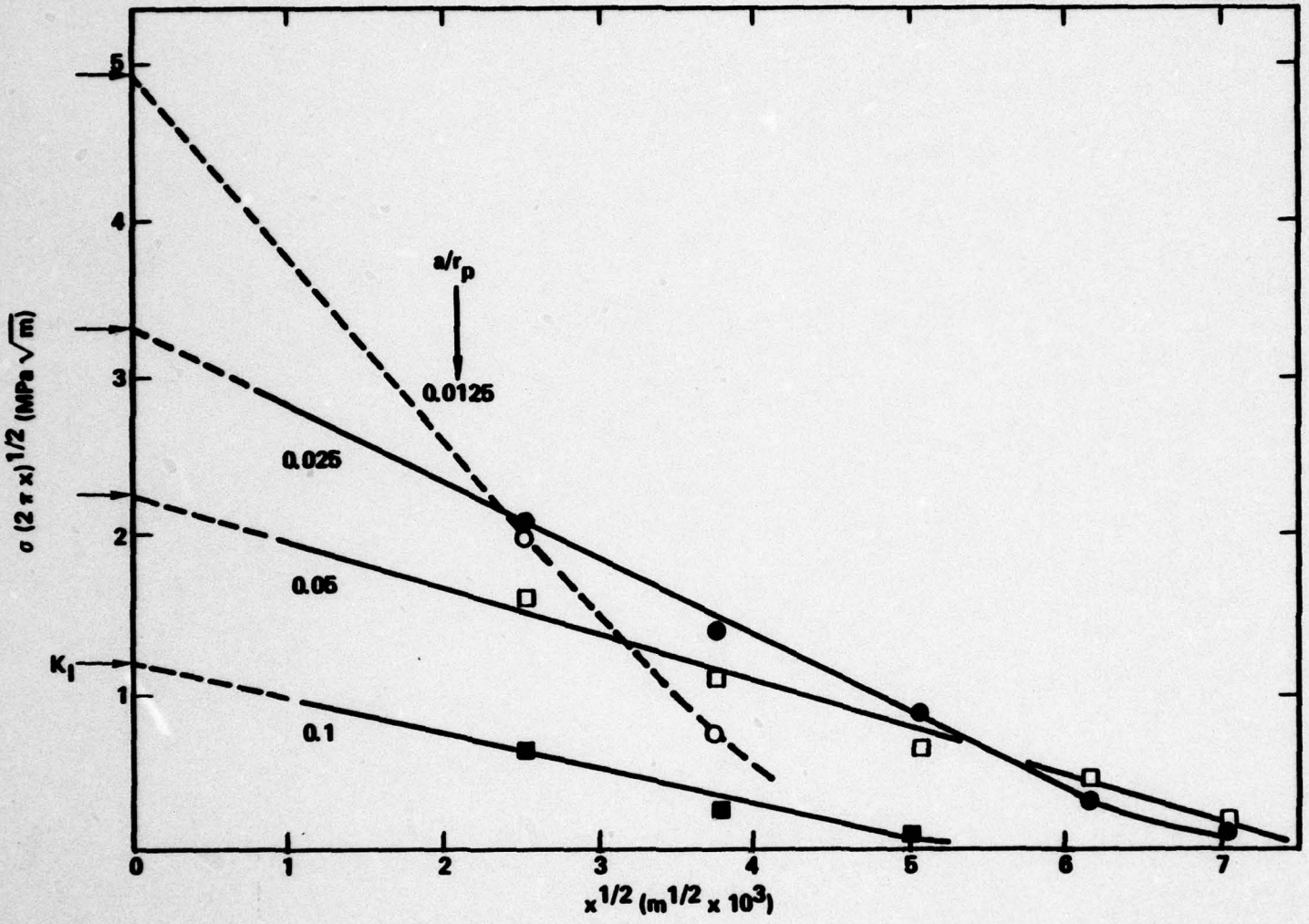

Fig. 7: The crack tip stress field results used to obtain the maximum stress intensity factors for cracks located at $r/\hat{r} = 1.5$.

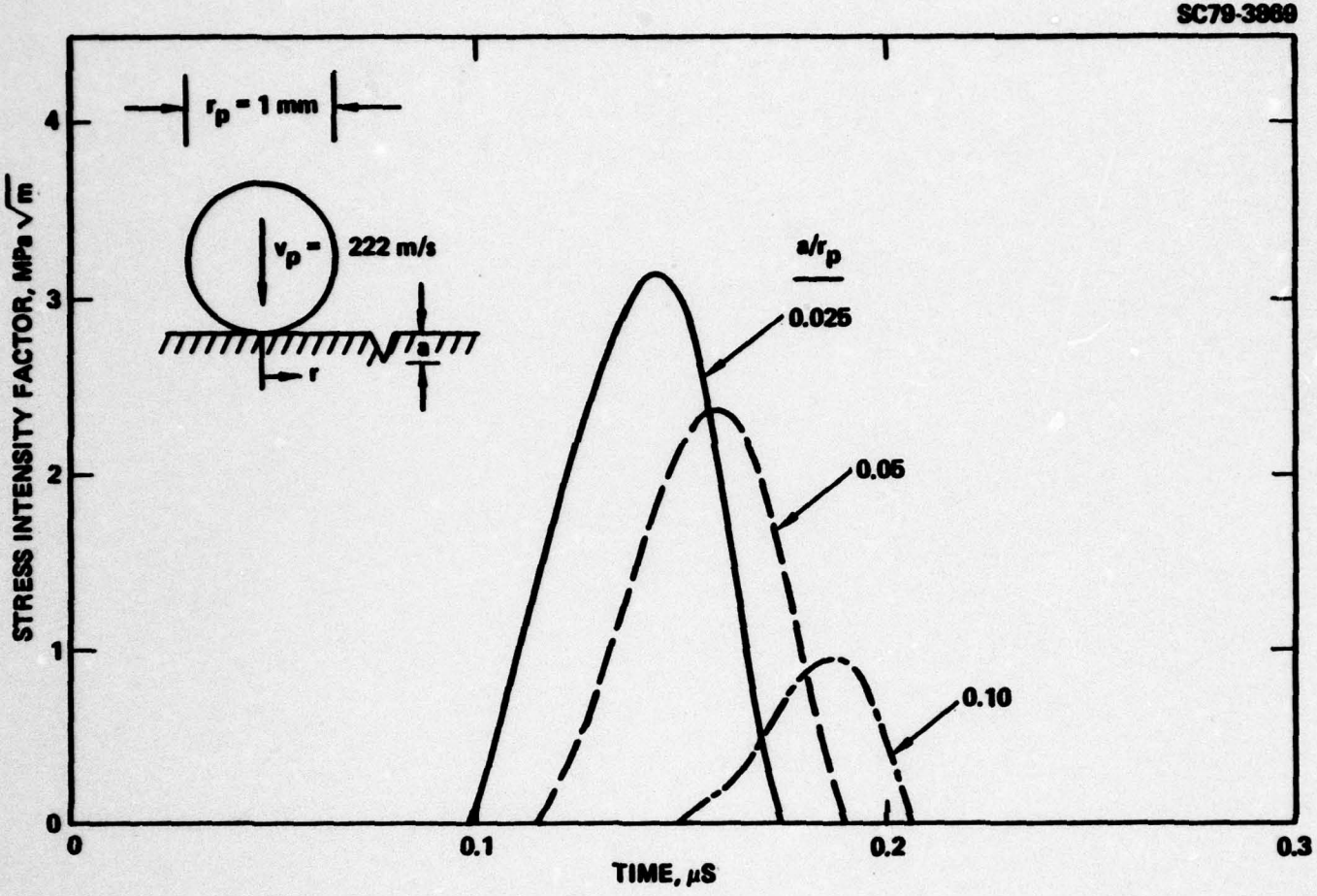

Fig. 8: The time dependence of the stress intensity factor for three crack lengths, for cracks located at $r/\hat{r} = 1.5$.

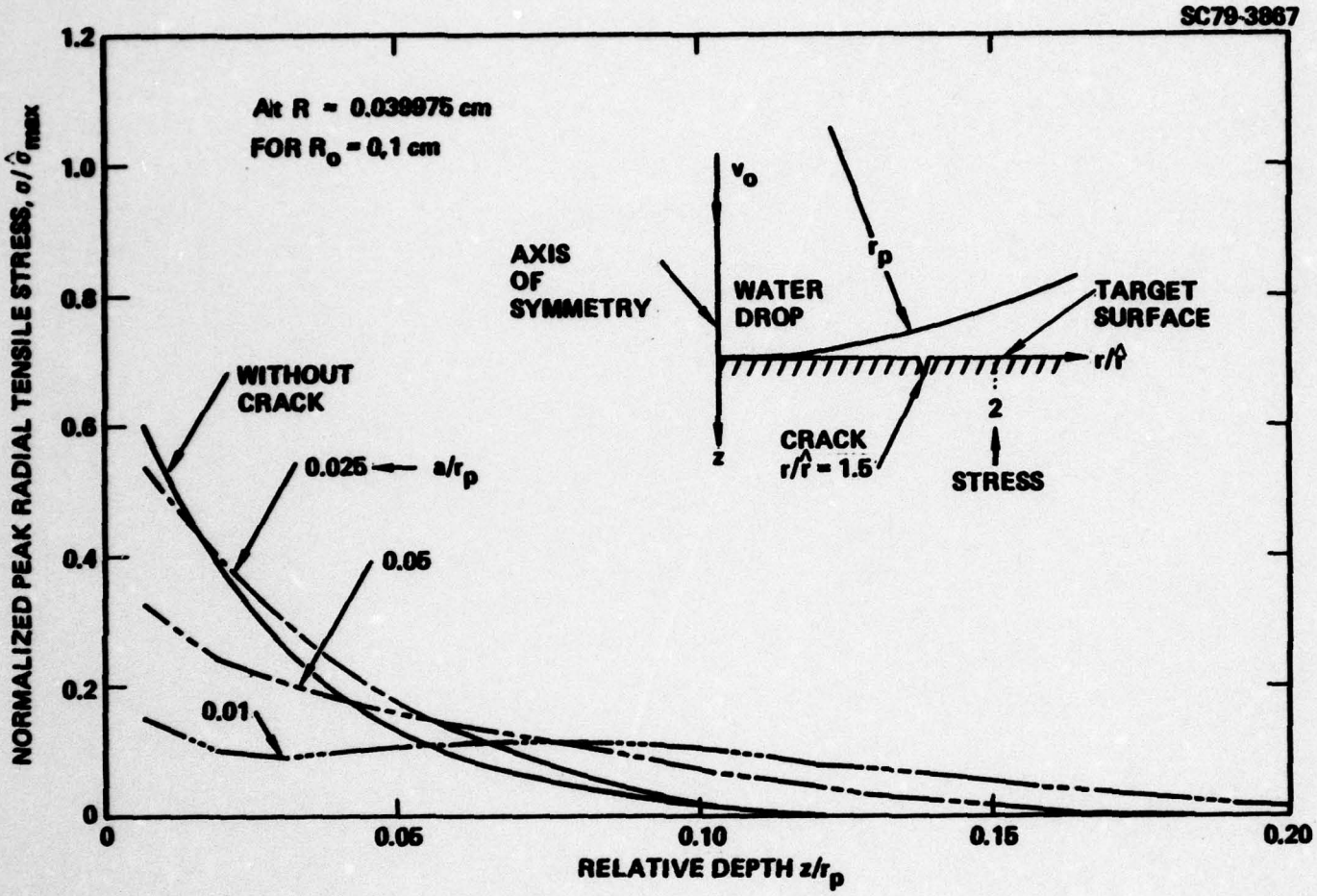

Fig. 9: The stresses computed at a radial location $r/\hat{r} = 2$ for a crack positioned at $r/\hat{r} = 1.5$.

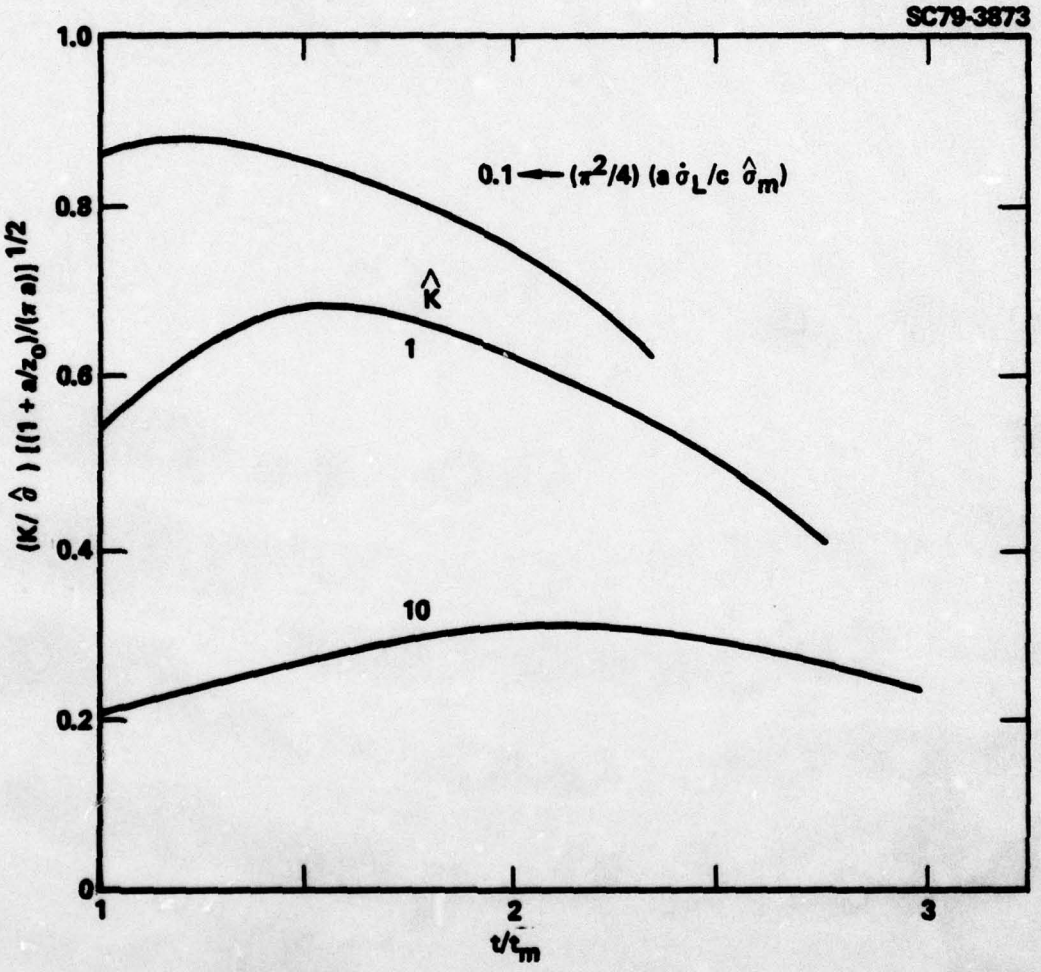

Fig. 10: Analytic solutions for the time dependence of the stress intensity factor.

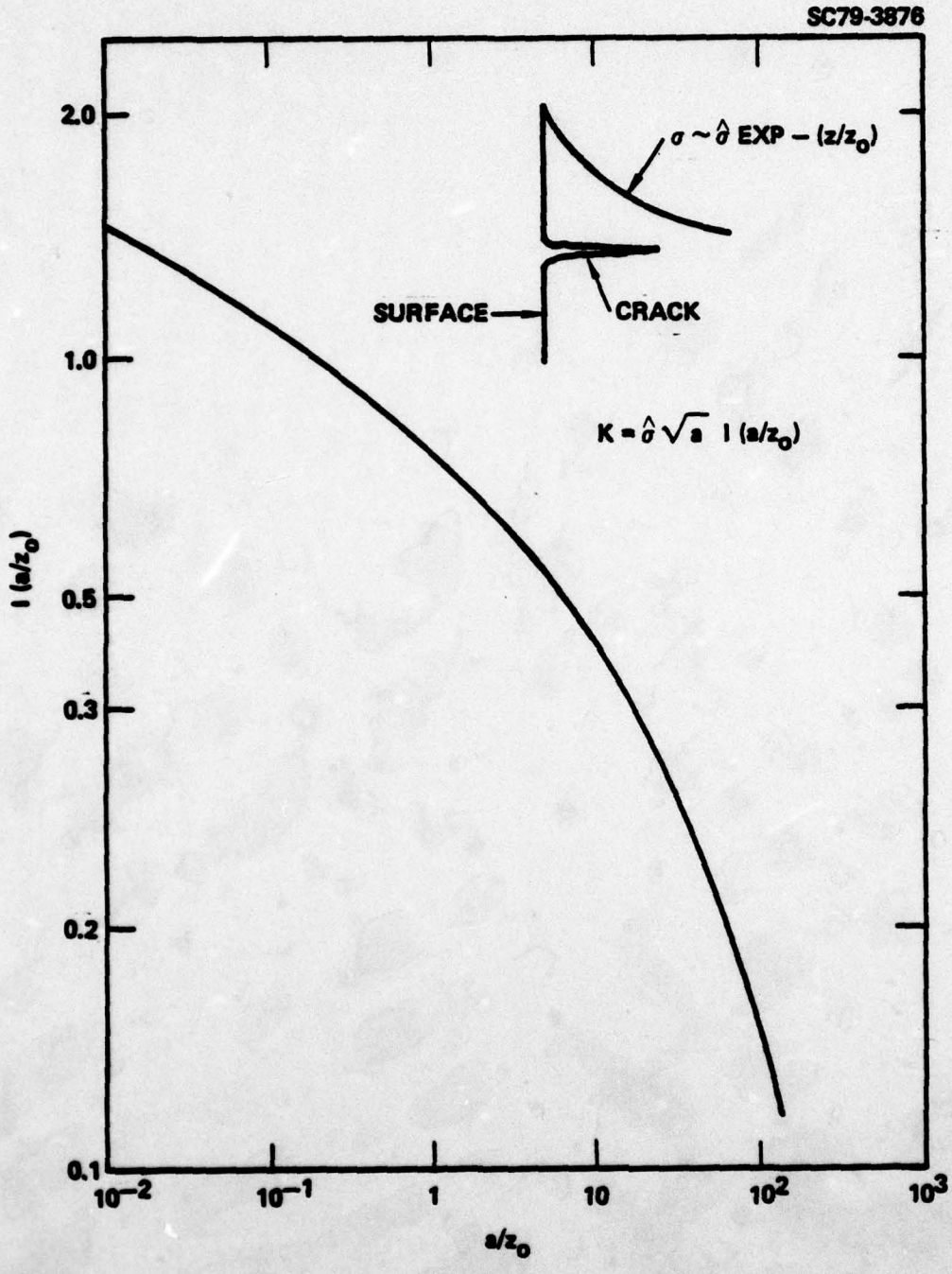

Fig. 11: The influence of the stress gradient on the quasi-static stress intensity factor.

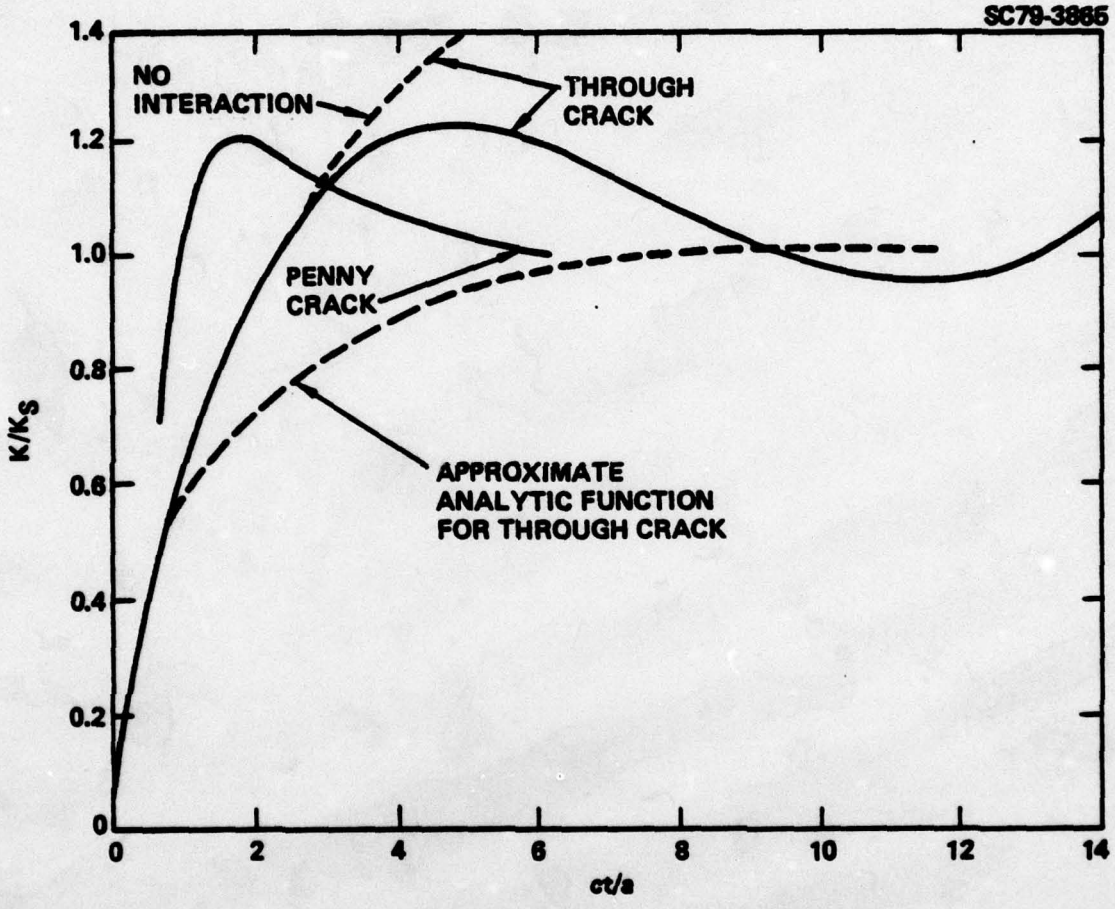

Fig. 12: The time dependence of the stress intensity factor at surface cracks, plotted in the normalized form suggest by the analysis.

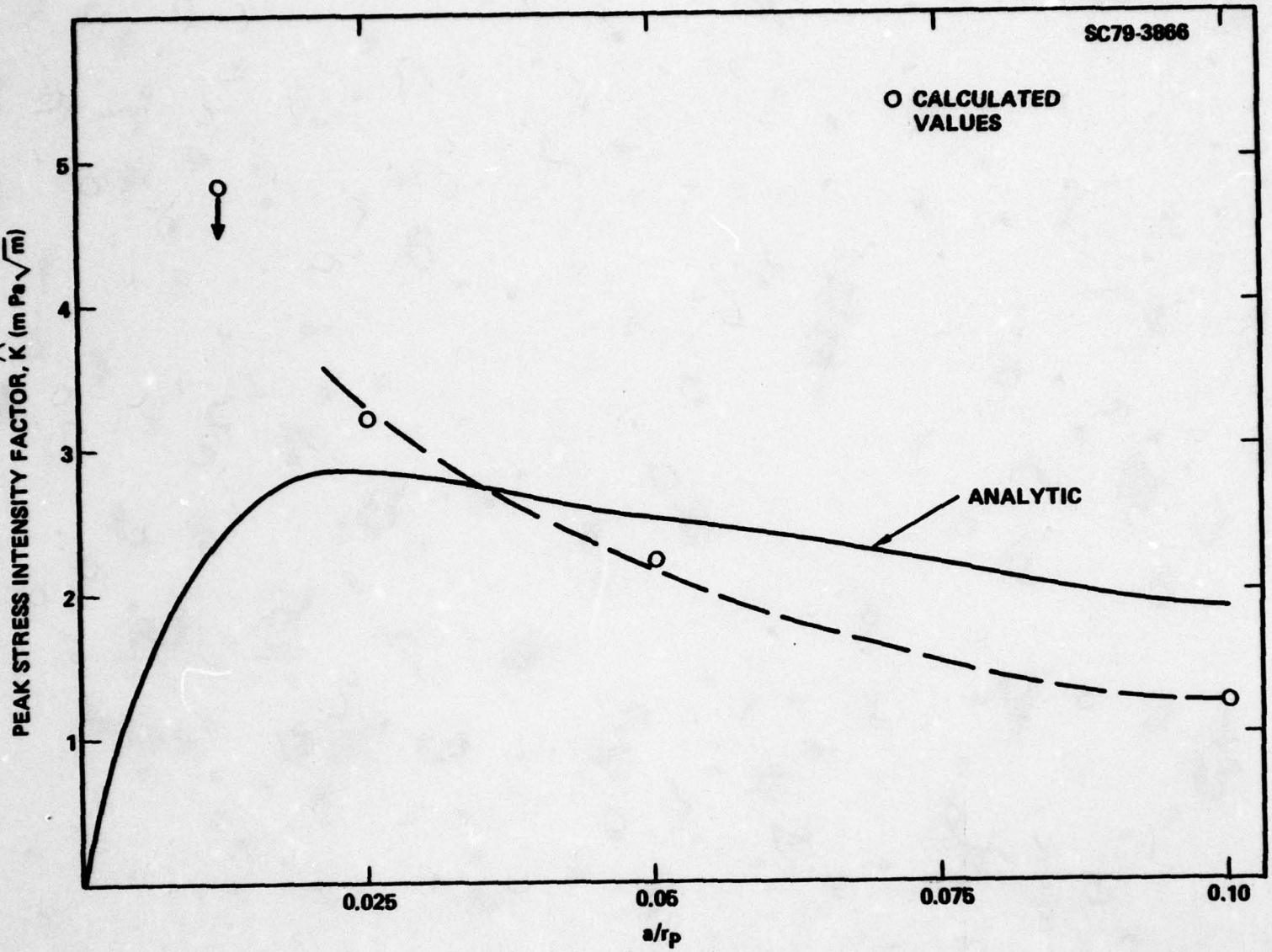

Fig. 13: A comparison of the variations of the peak stress intensity factor $\hat{K}$ with crack length a predicted by the analysis with the values determined by numerical computation.